Environmental impact analysis of surface printing and 3D inkjet printing applications using an imine based covalent organic framework: A life cycle assessment study

Juan J. Espada [a,*], Rosalía Rodríguez [a], Alejandro de la Peña [b], Mar Ramos [b], José L. Segura [c], Esther M. Sánchez-Carnerero [b]

[a] *Department of Chemical, Energy and Mechanical Technology. ESCET, Universidad Rey Juan Carlos, 28933, Móstoles, Madrid, Spain*
[b] *Department of Chemical and Environmental Technology. ESCET, Universidad Rey Juan Carlos, 28933, Móstoles, Madrid, Spain*
[c] *Departamento de Química Orgánica. Facultad de Ciencias Químicas, Universidad Complutense de Madrid, Avda. Complutense s/n, 28040, Madrid, Spain*

ARTICLE INFO

ABSTRACT

Covalent organic frameworks (COFs) are emerging materials with structural modularity that allows their application in many fields. The aim of this work is to determine the environmental impact of using an imine based covalent organic framework **(RT-COF-1)** for both surface printing (Case A) and 3D inkjet printing (Case B) by applying Life Cycle Assessment (LCA) methodology. Experimental data on **RT-COF-1** synthesis as well as results obtained by simulation of their precursors production, 1,3,5-tris-(4-aminophenyl) benzene (**TAPB**) and 1,3,5-benzenetricarbaldehyde (**BTCA**), are used. LCA results show that monomer synthesis is the most important contributor to environmental impacts in both case studies. On the other hand, the contribution of solvents used in Case A is also remarkable. The comparison between both case studies indicates that the environmental impacts of Case B is lower than that of Case A (reduction within 5%–65%). Finally, LCA results of Case B are compared to other materials used for 3D-printing, such as polymerizable ionic liquids (PILs). The results show that **RT–COF–1** compares favourably with PILs in five of nine impact categories, being especially relevant the reductions achieved in the abiotic depletion and acidification potential (>90%), in the primary energy consumption (~35%) and carbon footprint (~50%), suggesting the potential of **RT–COF–1** as 3D-printing material from an environmental perspective. This work is a first step for further research to highlight the main environmental burdens of using COF-based materials in this application.

1. Introduction

Covalent organic frameworks (COFs), constructed from small building blocks via covalent linkage, are emerging as a new class of 2D or 3D materials with high crystallinity, regular pores, low density and high surface areas (Côté et al., 2005; Diercks and Yaghi, 2017; El-Kaderi et al., 2007; Li et al., 2020). These properties, along with the diversity of building blocks and covalent linkage topology schemes, make COFs suitable materials to be used in a wide variety of fields such as adsorption and separation**,** catalysis, energy storage, semiconductor and optoelectronic, luminescence and sensors, mass transport, environmental remediation, biomedical applications, etc. (Geng et al., 2020; Guan et al., 2020; Li et al., 2020). However, most of these applications are limited by the lack of methodologies to process and integrate these materials on supports. In this regard, some advances have been made in producing thin-films of COFs on several surfaces (Colson et al., 2011; Medina et al., 2014), but only few cases allowed the preparation of microarrays of COFs on rigid SiO₂ surfaces, and flexible substrates (Colson et al., 2015; De la Peña Ruigómez et al., 2015). Recently, easier, smoother and faster synthetic procedures have been developed for the production of supported COFs (Li et al., 2020; Rodríguez-San-Miguel and Zamora, 2019; Wang et al., 2019), leading to the possibility of implementing COFs in novel applications. Nevertheless, processing challenges related to their limited capability for patterning must be overcome. In this regard, printing technologies (inkjet and 3D) appear as promising approaches to construct complex geometries, increasing the applications of COFs in different fields, since they allow integrating molecular bodies into devices keeping their precise microstructures

---

* Corresponding author.
  E-mail address: juanjose.espada@urjc.es (J.J. Espada).

described at atomic level (Mohammed et al., 2020). These technologies are included into Additive Manufacturing (AM) based on the layer-by-layer technique to design parts of complex geometry, using print head, nozzle or another printer technology (Muñoz et al., 2021). Among its advantages over conventional techniques, it must be noticed the geometrical customization, which leads to product flexibility and design freedom, reducing production time (Bikas et al., 2019). Currently, the versatility of AM to effectively produce complex structures using different materials has made this technology to grow in different manufacturing sectors (Agrawal, 2021). Furthermore, this manufacture allows reducing chemical and energy consumption, improving the environmental performance of the entire product life cycle (Maciel et al., 2019; Saade et al., 2020). In this regard, inkjet printing is a low-cost technology that allows developing thin films and patterns of high quality, making their manufacturing easier and simultaneously reducing consumption of energy and raw materials (Karami et al., 2022).

In this sense, de la Peña Ruigómez et al. (2015) reported a crystalline laminar imine-based COF (**RT–COF–1**) synthesized through Schiff reaction between two trigonal building blocks: 1,3,5-tris(4-aminophenyl) benzene (**TAPB**) and 1,3,5-benzenetricarbaldehyde (**BTCA**). This reaction can be conducted rapidly at room temperature and ambient pressure, unlike other imine-based polymers that require high temperature and pressure in a glass ampoule. These authors reported the possibility of using this **RT–COF–1** for inkjet printing (De la Peña Ruigómez et al., 2015), in which precise volumes of ink are deposited on a substrate (Teo et al., 2020; Zawadzki et al., 2022). The approach used by De la Peña Ruigómez et al. (2015) consists of using a premixed solution of **TAPB** and **BTCA** in DMSO in a single printhead, obtaining COF layers printed on acetate paper and SiO_2 surfaces. The printer used allows to create and define patterns over an area of 200×300 mm and handle substrates until 25 mm thick with adjustable Z height (De la Peña Ruigómez et al., 2015). This approach presents, among other disadvantages, that it requires high printing velocity to avoid solidification of the solution as well as large chemical consumption. Recently, Teo et al. (2021) have developed an inkjet-based procedure using in-air coalescence inkjet printer to produce COF with any shape in short time, obtaining successful results for **RT–COF–1**. These authors built an inkjet printer based on droplet collision capable to print a wide variety of materials using multiple printheads. This procedure presents as main advantage the possibility of loading both monomers (**TAPB** and **BTCA**) in separate printheads, avoiding short printing windows and enhancing control over material ejection (Teo et al., 2021).

Current environmental concerns on industrial manufacture are focused on environmental impact (mainly those related to energy consumption and harmful emissions) produced by emerging technologies, such as additive manufacture, to determine their sustainability (Ma et al., 2018; Muñoz et al., 2021). Environmental impact is defined as the mass equivalent of a reference substance, that accounts for the largest proportion of emissions responsible of this impact. For instance, the climate change is quantified through the amount equivalent of CO_2, main compound of greenhouse gas emissions (Panagiotopoulou et al., 2022). There is a wide number of environmental impacts analyzed for manufacturing and production sector, such as climate change, eutrophication, acidification, ozone depletion, human and ecotoxicity as well as the use of resources (Panagiotopoulou et al., 2022; Stavropoulos and Panagiotopoulou, 2022). The assessment of environmental impacts requires a comprehensive approach (from design step to end of life), and in this context Life Cycle Assessment (LCA) analysis is commonly used (Muñoz et al., 2021; Stavropoulos et al., 2016). LCA is a well stablished method to quantify direct and indirect environmental impacts related to products, processes and services. This method considers a holistic assessment of all life cycle steps: raw material extraction, manufacture, distribution, use and disposal/recycle/reuse of wastes (Athanasopoulou et al., 2018; Espada et al., 2021; Okoroafor et al., 2022; Rodríguez et al., 2018; Stavropoulos et al., 2016). As reported in literature, LCA has been

applied to identify the environmental impacts of AM for different sectors, such as automotive, aircraft and construction (Muñoz et al., 2021; Saade et al., 2020). LCA applications to inkjet printing have been reported for perovskite solar cells, showing that the electricity required for cell manufacture is the main contributor in most impact categories (Okoroafor et al., 2022). Cerdas et al. (2017) applied LCA to a 3D-printing-supported distributed manufacturing showing its potential benefits compared to a conventional centralized manufacturing system (Cerdas et al., 2017). Khosravani and Reinicke (2020) reported that energy consumption, waste material and air pollution are the most contributors to the environmental impact when using plastics as raw materials for 3D-printing (Khosravani and Reinicke, 2020). Maciel et al. (2019) analysed the environmental impact of 3D-polymerizable imidazolium-based ionic liquid (Maciel et al., 2019). This work, unlike others reported in the literature, presents a LCA analysis of several environmental impacts, including the synthesis of the monomers to obtain the ionic liquid, as well as sensitivity analysis of the most important variables. These authors concluded that the synthesis of monomers and the use of solvents are the most important contributors to the overall impacts. In addition, they showed the promising capabilities of PILs for additive manufacturing from an environmental point of view.

In this work, a COF-based material was selected because these materials have a wide range of applications related to environmental purposes, but studies on their sustainability are scarce. Therefore, it is of interest to stduy the applications of this type of materials through LCA method. The aim of this work is to determine the environmental performance of **RT–COF–1** for both surface and 3D inkjet printing (Cases A and B) by applying LCA. We chose **RT–COF–1** for the analysis because it can be rapidly synthesized in air at room temperature, making it suitable for both surface and 3D-printing (De la Peña Ruigómez et al., 2015). The synthesis of the monomers to obtain **RT–COF–1** was simulated based on experimental and literature data to quantify environmental inventory data. Thereafter, environmental impacts of both surface and 3D-printing processes were determined and discussed, and the best option was compared to other materials reported in the literature.

2. Methodology

2.1. Goal and scope of the LCA study

This study aims to determine the environmental performance of two different printing methods for **RT-COF-1** by applying LCA. Two case studies are analysed: surface COF printing (Case A) and 3D printing (Case B). Besides, the best alternative is compared to LCA results of other materials available in the literature (Maciel et al., 2019). Fig. 1 shows an overview of the process, including the involved steps. As can be observed, the synthesis of both monomers from commercial precursors to yield **RT-COF-1** was considered (blocks with green and blue lines), including all the steps involved in these pathways (explained in detail in sections below). Printing process (dotted orange line) includes the monomers previously synthesized, the solvents and the energy used in each case (Case A: both monomers are mixed in a single cartridge; Case B: A single cartridge is used for each monomer).

2.2. Life cycle inventory analysis (LCIA)

2.2.1. LCA assumptions

The following assumptions were made in both case studies:

- Synthesis of both monomers were taken from pathways available in the literature and simulated to obtain mass and energy balances (see explanation in further sections).
- All the inputs and outputs of the processes were considered within the system boundaries.
- Wastes generated in the process were disposed as hazardous materials in an underground deposit.
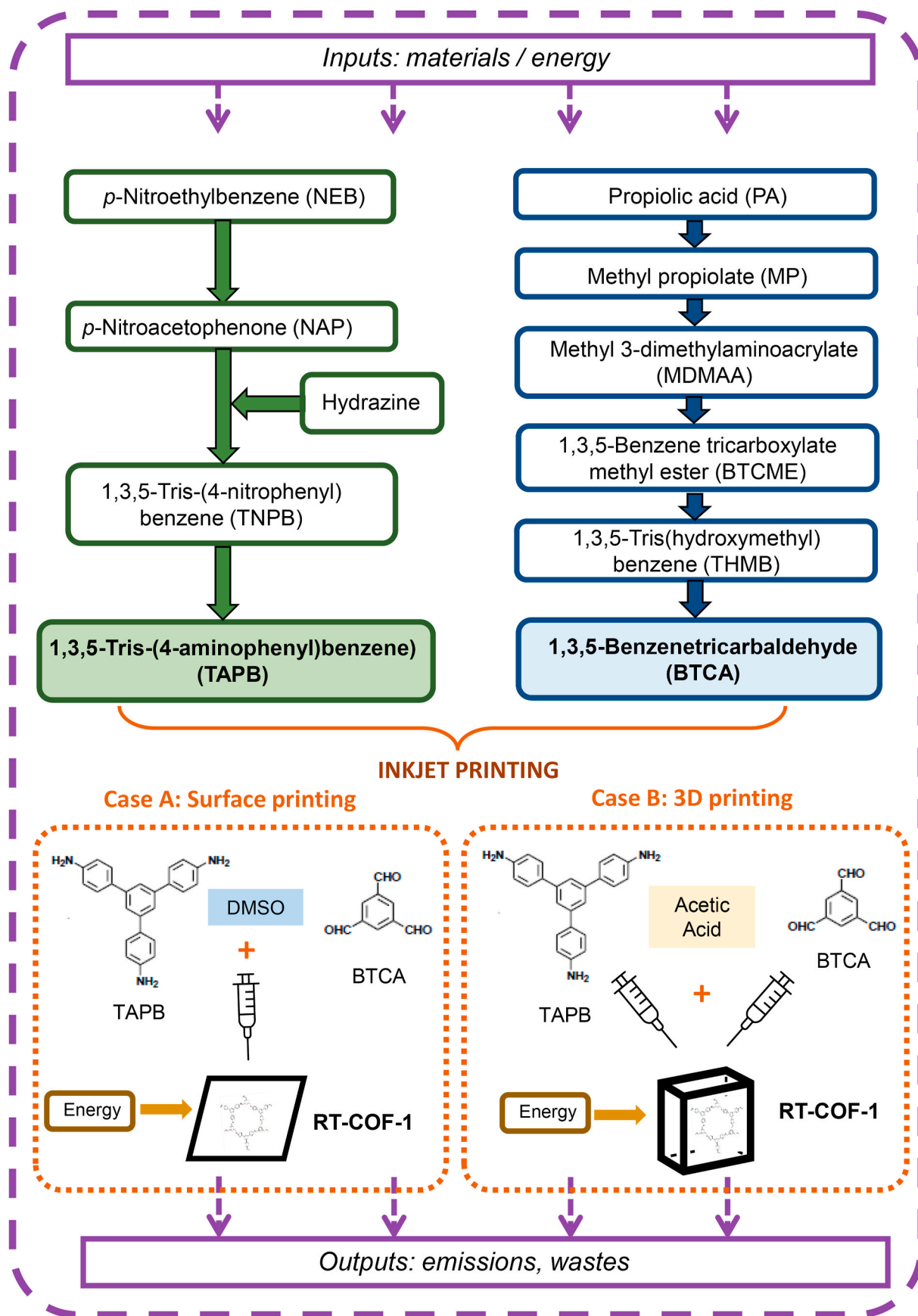
Fig. 1. Boundary limits considered for both case studies. Synthesis of monomers (blocks with blue and green line); printing process (dotted orange line). Limits of the system (purple dashed line). (For interpretation of the references to colour in this figure legend, the reader is referred to the Web version of this article.)

- It was supposed that solvents were recovered, whereas capital goods are excluded of the study.
- The functional unit considered in the present work was 1 g of **RT-COF-1** printed for both case studies.

2.2.2. Data collection

To obtain inventory data, each step of **RT-COF-1** synthesis was simulated using SuperPro Designer 9.5 (Intelligen Inc. Scotch Plains, NJ, USA) as described below. The synthesis of the imine-linked covalent organic framework (**RT-COF-1**) at room temperature is based on Schiff reaction between two trigonal building blocks, 1,3,5-tris(4-amino-phenyl)benzene (**TAPB**) and 1,3,5-benzenetricarbaldehyde (**BTCA**) (De la Peña Ruigómez et al., 2015). Due to the lack of data on monomer manufacture processes in the LCA inventory database used in this work, they were simulated using SuperPro Designer 9.5 (Intelligen Inc. Scotch Plains, NJ, USA), as shown in the flowsheet diagrams (Figs. S1 and S2, available in the supplementary material). For this purpose, well-known reactions were used according to experimental data on **RT-COF-1** synthesis, including all the required separation steps. Mass and energy balances were solved to quantify the life cycle inventory data of the process and in all cases, it was supposed that solvent recovery was 99%. Primary processes for materials and energy production for each step were taken from database (Ecoinvent 3.8) along with Gabi 10.6 (Sphera Solutions GmbH. Leinfelden-Echterdingen, Germany). Finally, heating was supposed to be obtained from natural gas, whereas Spanish electric mix 2022 was used for electricity production.

2.2.2.1. Synthesis of 1,3,5-tris(4-aminophenyl) benzene (TAPB). The reactions and the pathway of **TAPB** synthesis used in the simulation of the process are shown in Table 1. The simulation of each step is described below.

i) Synthesis of p-nitroethylbenzene (NEB). The first step in the synthesis of **TAPB** was the nitration of ethylbenzene. In a reactor, concentrated nitric and sulfuric acid were added to ethylbenzene over 6 h, keeping the temperature below 40 °C. After the addition, the mixture was heated at 100 °C for 4 h according to the procedure reported in the literature (Table 1, entry 1). When the reaction was complete, the product was washed with water and aqueous sodium hydroxide and decanted to remove excess acid. Finally, the product was distilled to obtain **NEB**. The remaining ethylbenzene was separated in a distillation column and recycled to the process.

ii) Synthesis of p-nitroacetophenone (NAP). The obtained **NEB** was then oxidized with CrO_3 using air and thereafter, the mixture was cooled and washed with aqueous sodium carbonate. The stream containing **NAP** was distilled (Table 1, entry 2) and the recovered **NEB** was recycled to the process.

iii) 1,3,5-Tris-(4-nitrophenyl) benzene (TNPB). **NAP** was self-condensed induced by $SiCl_4$ in ethanol to produce **TNPB** (Table 1, entry 3). **NAP** dissolved in absolute ethanol at 0 °C was mixed with $SiCl_4$ and the resulting stream was stirred. Ethanol was recovered by distillation as shown in the flowsheet diagram (see Fig. S1 in supplementary

material). The resulting downstream was cooled and stirred with saturated ammonium chloride solution in a blending tank. The obtained precipitate was filtered, dried, and dissolved in ethanol. The excess of ethanol was recovered by distillation and reused in the process.

iv) Synthesis of 1,3,5-tris(4-aminophenyl) benzene (TAPB). Subsequently, **TNPB** was reduced with hydrazine in presence of Pd/C catalyst to yield the target C_3-symmetrical amine, **TAPB** in 80% yield over two steps (Table 1, entry 4). The synthesis of hydrazine (reducing agent) was simulated following the described procedure (Table 1, entry 5). According to this reaction, aqueous ammonia, gelatine solution and sodium hypochlorite solution were heated at 120 °C. The mixture was transferred to another reactor and concentrated sulfuric acid was added. The mixture was then filtered, and the precipitate was washed with cold ethanol. To obtain higher purity of hydrazine, the stream was dissolved in hot water and recrystallized, filtered, and dried. Purified hydrazine was used in the reduction of **TNPB**, and the resulting stream was filtered and dried, obtaining **TAPB** monomer.

The results obtained by simulation for all the steps involved in **TAPB** synthesis are detailed in supplementary material (Table S1).

2.2.2.2. Synthesis of 1,3,5-benzenetricarbaldehyde (BTCA). Reactions and pathway used in the simulation of **BTCA** synthesis are shown in Table 2.

i) Synthesis of propiolic acid (PA). **BTCA** monomer production started with the synthesis of **PA** from acetylene under basic conditions using a cooper catalyst (Table 2, entry 1). According to this procedure, acetylene and cooper catalyst were mixed in DMSO under basic conditions. To obtain the basic medium, an ammonia stream (recovered downstream) was recirculated to the process (see Fig. S2 in supplementary material). Then, a stream of CO_2 was bubbled through the reaction mixture. After reaction time, gases were released, and acetylene was recovered. HCl 30% was added to the mixture until acidic pH was reached and the product was extracted with ethyl acetate. After decanting the mixture, **PA** was obtained, and ethyl acetate was recovered by distillation.

ii) Synthesis of methyl propiolate (MP). The obtained **PA** was dissolved in methanol and heated under reflux for 1h with concentrated sulfuric acid (Table 2, entry 2). The mixture was extracted with diethyl ether, washed with brine and **MP** was isolated after distillation.

iii) Synthesis of methyl 3-dimethylaminoacrylate (MDMAA). **MP** was then dissolved in diethyl ether and the solution was cooled down. A stream of dimethylamine was passed through the cold mixture yielding **MDMAA** according to the procedure (Table 2, entry 3).

iv) Synthesis of 1,3,5-benzene tricarboxylate methyl ester (BTCME). **BTCME** was obtained by trimerization of the enamine obtained under acidic conditions (Table 2, entry 4). The trimerization reaction was carried out by mixing **MDMAA** in 1,2-dimethoxyethane with sulfuric acid. The mixture was cooled, extracted with ethyl acetate, and separated by decanting. After recovering the solvent by distillation, **BTCME** was obtained.

v) Synthesis of 1,3,5-tris(hydroxymethyl)benzene (THMB). The C_3-symmetrical ester was reduced with $LiAlH_4$ in anhydrous diethyl ether,

Table 1
Reactions considered for **TAPB** synthesis.

Entry	Substance	Reaction	Yield	Reference
1	NEB ($C_8H_9NO_2$)	$C_8H_{10} + HNO_3 \rightarrow C_8H_9NO_2 + H_2O$	32%	Cline and Emmet Reid (1927)
2	NAP ($C_8H_7NO_3$)	$C_8H_9NO_2 + CrO_3 + \frac{1}{4} O_2 \rightarrow C_8H_7NO_3 + \frac{1}{2} Cr_2O_3 + H_2O$	10%	Emerson et al. (1946)
3	TNPB ($C_{24}H_{15}N_3O_6$)	$3\ C_8H_7NO_3 + 3/2\ SiCl_4 \rightarrow C_{24}H_{15}N_3O_6 + 3/2\ SiO_2 + 6\ HCl$	–	Bao et al. (2006)
4	TAPB ($C_{24}H_{21}N_3$)	$C_{24}H_{15}N_3O_6 + 9/2\ N_2H_4 \rightarrow C_{24}H_{21}N_3 + 6\ H_2O + 9/2\ N_2$	80% (over two steps)	Bao et al. (2006)
5	Hydrazine (N_2H_4)	$NaOCl + 2\ NH_3 \rightarrow N_2H_4 + H_2O + NaCl$	10%	Adams and Brown (1941)

Table 2
Reactions considered for **BTCA** synthesis.

Entry	Substance	Reaction	Yield	Reference
1	PA ($C_3H_2O_2$)	$C_2H_2 + CO_2 \rightarrow C_3H_2O_2$	40%	Díaz Velázquez et al. (2017)
2	MP ($C_4H_4O_2$)	$C_3H_2O_2 + CH_3OH \rightarrow C_4H_4O_2 + H_2O$	60%	Baldwin and Black (1984)
3	MDMAA ($C_6H_{11}NO_2$)	$C_4H_4O_2 + C_2H_7N \rightarrow C_6H_{11}NO_2$	100%	Irlapati et al. (2003)
4	BTCME ($C_{12}H_{12}O_6$)	$3\ C_6H_{11}NO_2 \rightarrow C_{12}H_{12}O_6 + 3\ C_2H_7N$	60%	Arava et al. (2011)
5	THMB ($C_9H_{12}O_3$)	$C_{12}H_{12}O_6 + H_4LiAl + 8\ H_2O \rightarrow C_9H_{12}O_3 + 3\ CH_3OH + LiOH + Al(OH)_3 + 2\ H_2$	73%	Xu et al. (2018)
6	BTCA ($C_9H_6O_3$)	$C_9H_{12}O_3 + C_5H_6NClCrO_3 + 3/4\ O_2 \rightarrow C_9H_6O_3 + C_5H_6NCl + \frac{1}{2}\ Cr_2O_3 + 3\ H_2O$	53%	Xu et al. (2018)
7	PCC ($C_5H_6NClCrO_3$)	$CrO_3 + HCl + C_5H_5N \rightarrow C_5H_6NClCrO_3$	84%	Corey and Suggs (1975)
8	Pyridine (C_5H_5N)	$2\ C_2H_4O + CH_2O + NH_3 \rightarrow C_5H_5N + 3\ H_2O + H_2$	33%	Shimizu et al. (1998)

and the obtained mixture was cooled down to room temperature in presence of sulfuric acid and methanol. Excess acid was neutralized with ammonium hydroxide and the mixture was filtered and washed with methanol. The corresponding alcohol was isolated by extraction with ethyl acetate (Table 2, entry 5).

vi) Synthesis of 1,3,5-benzenetricarbaldehyde (BTCA). Subsequently, **THMB** was oxidized with pyridinium chlorochromate (PCC) to obtain the target trigonal building block, **BTCA** (Table 2, entry 6). The oxidation reaction was performed with **THMB** and PCC in dichloromethane at room temperature. The oxidizing reagent, PCC, was prepared from chromium trioxide and pyridine in acidic media (Table 2, entry 7). Pyridine synthesis was carried out by loading a reactor with a zeolite catalyst along with a mixture of acetaldehyde and formaldehyde vaporized with ammonia stream keeping the reactor at 450 °C (Table 2, entry 8). Then, pyridine was reacted with hydrochloric acid and CrO₃. The obtained solution was cooled at 0 °C, and after filtration, PCC was obtained in 84% yield (Corey and Suggs, 1975). The obtained PCC was

used in the oxidation reaction of **THMB** in dichloromethane. After reaction, the mixture was filtered and washed with dichloromethane, hydrochloric acid, sodium bicarbonate and water. The target **BTCA** monomer was obtained after recrystallization from ethyl acetate and the solvents were recovered by distillation (Xu et al., 2018).

The results obtained by simulation for all the steps involved in **BTCA** synthesis are detailed in supplementary material (Table S2).

2.2.2.3. Inkjet printing. From **TAPB** and **BTCA** monomers, **RT–COF–1** can be synthesized following the pathway shown in Table 3.

This reaction can be conducted following two approaches depending on the printing type (De la Peña Ruigómez et al., 2015; Teo et al., 2021).

A) Surface printing. In this case, RT–COF–1 layers are inkjet printed on acetate paper by premixed solution in a single printhead (De la Peña Ruigómez et al., 2015). To obtain the **RT-COF-1** printed piece (1 g) a printer with piezoelectric inkjet technology was used. The ink was prepared by dissolving stoichiometric amounts of monomers (**TAPB** and

Table 3
Synthesis and pathway for **RT-COF-1** synthesis.

Entry	Substance	Reaction	Yield	Reference
1	RT–COF–1 ($C_{33}H_{21}N_3 \cdot 2.5\ H_2O$)	$C_{24}H_{21}N_3 + C_9H_6O_3 \rightarrow C_{33}H_{21}N_3 \cdot 2.5\ H_2O + \frac{1}{2}\ H_2O$	96%	De la Peña Ruigómez et al. (2015)

BTCA) using DMSO as solvent in the same cartridge (see Fig. 1). The resulting printed piece was washed with methanol, and the mixture of solvents (DMSO and methanol) was separated and recovered. Amounts of **TAPB** and **BTCA** monomers were calculated from **RT-COF-1** synthesis yield above shown in Table 3. To calculate energy requirements of **RT-COF-1** synthesis, it was simulated according to the experimental data reported by De la Peña Ruigómez et al. (2015), as shown in Fig. S3 (supplementary material). Electricity consumed by printing process was calculated from technical specifications of the printer (Fujifilm, 2013). The detailed input and outputs of the process are summarized in supplementary material (Table S3).

B) 3D-printing. 3D COF-based monoliths can be obtained using in-air coalescence and reaction of inkjet printed monomer droplets (Teo et al., 2021). In this case, each monomer is placed in separate cartridges along with acetic acid. The resulting COF piece is washed with THF, as reported by these authors. This innovative strategy presents some advantages, avoiding the short printing window through the separate monomers. In addition, this approach offers a microscopic control over material ejection and customization by allowing the tailoring of different geometry of COFs on substrates (Teo et al., 2021). The procedure is illustrated in Fig. 1.

2.3. Environmental impact assessment (EIA)

The evaluation of environmental impacts for both cases A and B was performed by using the mid-point approach. The impact categories were selected according to other works on LCA of 3D-printing materials reported in the literature (Maciel et al., 2019). Cumulative Energy Demand (CED) was calculated to quantify the direct and indirect primary energy use throughout the life cycle (Huijbregts et al., 2010). In addition, Abiotic Depletion Potential (ADP), Acidification Potential (AP), Eutrophication Potential (EP), Fresh Water Aquatic Ecotoxicity Potential (FAETP), Global Warming Potential (GWP), Human Toxicity Potential (HTP), Marine Aquatic Ecotoxicity Potential (MAETP) and Ozone Layer Depletion Potential (OLDP) were selected and quantified by using CML 2001–Aug.2016 methodology, same as other works (Maciel et al., 2019) to compare LCA results.

3. Results and discussion

3.1. Synthesis of monomers

Table 4 shows the LCA results obtained for the synthesis of monomers (**TAPB** and **BTCA**). As can be observed, the impact values for **BTCA** are clearly higher than those ones for **TAPB** in all categories due to the large amounts of resources (materials and energy) as well as processes needed for its synthesis.

Fig. 2 depicts the contribution analysis of the steps involved in the synthesis of the monomers. As shown, in the case of the **TAPB**, the synthesis of hydrazine is the most important contributor in all

Table 4
LCA results for the synthesis of monomers referred to FU (1 g of **RT-COF-1**).

Impact category	TAPB	BTCA
Cumulative Energy Demand, CED (MJ)	3.00E-01	7.11E-01
Abiotic Depletion Potential, ADP (kg Sb-eq)	2.58E-07	2.01E-06
Acidification Potential, AP (kg SO_2-eq)	4.04E-05	1.27E-04
Eutrophication Potential, EP (kg PO_4-eq)	2.30E-05	1.18E-04
Fresh Water Aquatic Ecotoxicity Potential, FWAEP (kg 1,4 DCB-eq)[a]	2.96E-03	4.11E-03
Global Warming Potential, GWP (kg CO_2-eq)	1.09E-02	2.89E-02
Human Toxicity Potential, HTP (kg 1,4 DCB-eq)[a]	3.27E-03	5.85E-03
Marine Aquatic Ecotoxicity Potential, MAEP (kg 1,4 DCB-eq)[a]	8.09E+00	9.98E+00
Ozone Layer Depletion Potential, OLDP (kg CFC-11-eq)[b]	5.93E-10	5.56E-08

[a] DCB: Dichlorobenzene.
[b] CFC: Trichlorofluoromethane.

categories, except AD and OLDP, in which the palladium catalyst and the synthesis of **TNPB** (**TAPB** precursor) are, respectively, the largest contributors. In the case of hydrazine, the most important factor is the waste disposal because of the low yield of this reaction (see Table 1), which implies the use of large amount of chemicals and therefore, the impact increases. On the other hand, palladium catalyst is the most important contributor to AD, since the extraction of the metal affects resource depletion. Finally, the synthesis of **TNPB** is the main responsible of OLDP impact due to silicon tetrachloride production, which causes halogenated emissions. Regarding the synthesis of the monomer **BTCA**, the most important contributor to all impact categories is the production of its precursor (**THMB**), except for OLDP, in which the production of dichloromethane (used to synthesise **BTCA**, see Table 2) shows the largest contribution because of halogenated emissions to air.

3.2. Printing processes

Table 5 shows the LCA results for **RT-COF-1** printed in case A and B in each impact category.

As can be observed, Case B is superior to Case A in all categories, showing remarkable differences in several of them. As reactions to obtain both monomers are the same, the main difference of the case studies is due to the printing process, as different materials (solvents) and energy are used.

Fig. 3 depicts the relative contribution of each step of the process for both case studies. As can be observed, the synthesis of both monomers (**TAPB** and **BTCA**) are the main contributors to most impact categories in both cases. On the other hand, it can be seen how the relative contribution of the solvents and energy used in the printing process is clearly larger in Case A, comprising >70% in some categories, such as AP. This result is linked to the different solvents (and their amount) used in Case A and B: DMSO and methanol (Case A) and acetic acid and THF (Case B). Among these solvents, DMSO is used in the largest amount (see Table S3 in the supplementary material), leading to high impacts due to its manufacture presents large environmental burdens. This fact also increases the energy consumed to separate solvents in Case A regarding to Case B (see Table S3 in the supplementary material), enlarging the impacts.

Energy consumed is a key factor to compare the environmental performance between different printing processes (Maciel et al., 2019). By analysing the most affected categories regarding to energy in Fig. 3, it can be observed that the largest contributions were observed for CED and GWP in both cases. Regarding to CED, power and heat consumed in Case A and B are similar (by 13%). In the same way, the greenhouse gas emissions generated by the production of this energy contributes by 15% to GWP in both cases. The main factors responsible of this contribution are the fossil resources of the Spanish electric mix and the combustion of natural gas needed for solvent separation.

3.2.1. Contribution analysis

In this section a detailed contribution analysis of the different steps to the overall inkjet printing processes (Cases A and B) is presented to identify the environmental burdens as well as their causes. Fig. 4 shows the results of this analysis, in which the steps with contributions <5% were grouped as "Others", distinguishing between those corresponding to the synthesis of monomers (**TAPB** and **BTCA**) and those due to the printing processes (excluding the contribution of the monomers) to make the identification of the environmental impacts easier.

The results obtained for CED show that DMSO used to dissolve the monomers in the ink cartridge exhibits the largest contribution in Case A. The production of this solvent requires large amount of energy and, despite 99% is recovered in the process, the amount needed to print 1 g of **RT-COF-1** is remarkably high (8.73 g). This fact along with the use of non-renewable energy resources for its manufacture, leads to the largest contribution to CED. On the contrary, the contribution of solvents in Case B is negligible due to acetic acid is used in less proportion (1.20 g/g
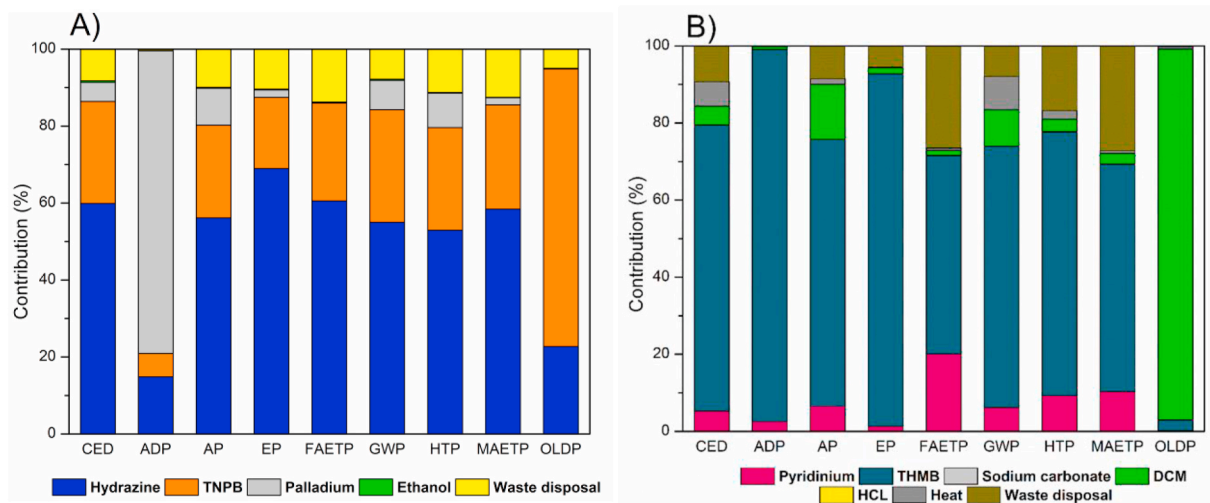
Fig. 2. Environmental breakdown of impacts related to monomers: A) **TAPB** and B) **BTCA**.

Table 5
LCA results for inkjet printing process referred to FU (1 g of printed **RT-COF-1**).

Impact category	Case A	Case B
Cumulative Energy Demand, CED (MJ)	1.72E+00	1.26E+00
Abiotic Depletion Potential, ADP (kg Sb-eq)	3.21E-06	2.28E-06
Acidification Potential, AP (kg SO_2-eq)	5.40E-04	1.84E-04
Eutrophication Potential, EP (kg PO_4-eq)	1.64E-04	1.44E-04
Fresh Water Aquatic Ecotoxicity Potential, FWAEP (kg 1,4 DCB-eq)[a]	1.02E-02	7.39E-03
Global Warming Potential, GWP (kg CO_2-eq)	6.15E-02	4.89E-02
Human Toxicity Potential, HTP (kg 1,4 DCB-eq)[a]	1.51E-02	9.96E-03
Marine Aquatic Ecotoxicity Potential, MAEP (kg 1,4 DCB-eq)[a]	2.66E+01	1.94E+01
Ozone Layer Depletion Potential, OLDP (kg CFC-11-eq)[b]	5.86E-08	5.65E-08

[a] DCB: Dichlorobenzene.
[b] CFC: Trichlorofluoromethane.

RT-COF-1) and the environmental impacts of its production are lower than those ones for DMSO.

On the other hand, the synthesis of **PA** involved in the synthesis of **BTCA** monomer, represents by 20% in both case studies due to the consumption of non-renewable resources for acetylene production (precursor of **PA,** see Table 2).

Results on ADP category indicate that **PA** is the most important contributor in Case A and B (by 60% and 80%, respectively). The main responsible of this impact is the large amount of copper used to synthesise **PA** (1.50 g/g BTCA monomer), which increases the consumption of non-renewable elements and therefore, ADP value raises.

Regarding AP, it can be observed differences between the main contributions in both study cases, as depicted in Fig. 4. In this sense, DMSO along with the **PA** presents the highest contribution in Case A (by
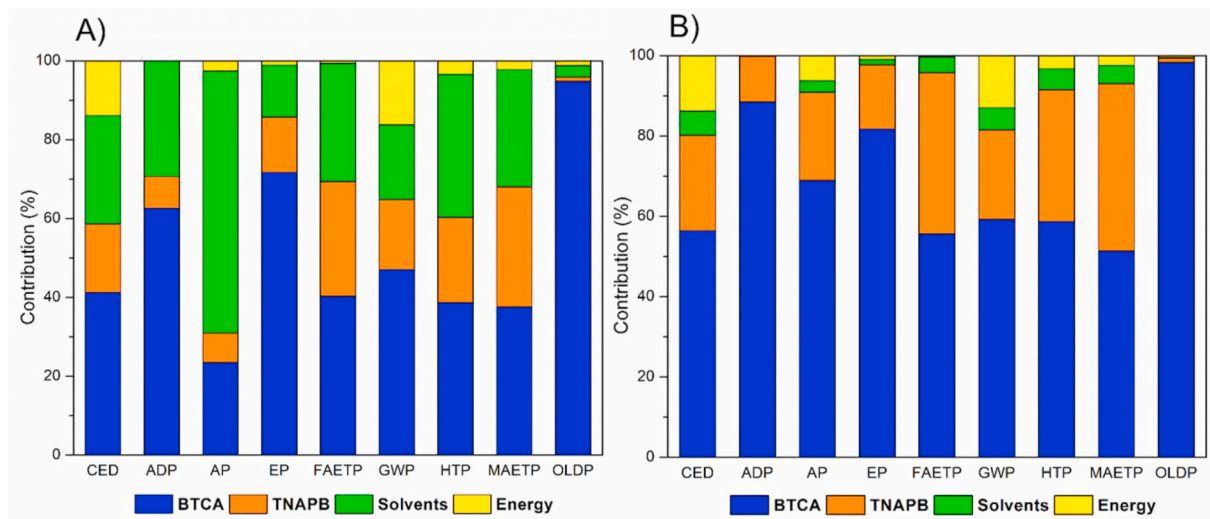

Fig. 3. Environmental impact contribution of the different steps involved in inkjet printing process for **RT-COF-1**: A) Case A and B) Case B.
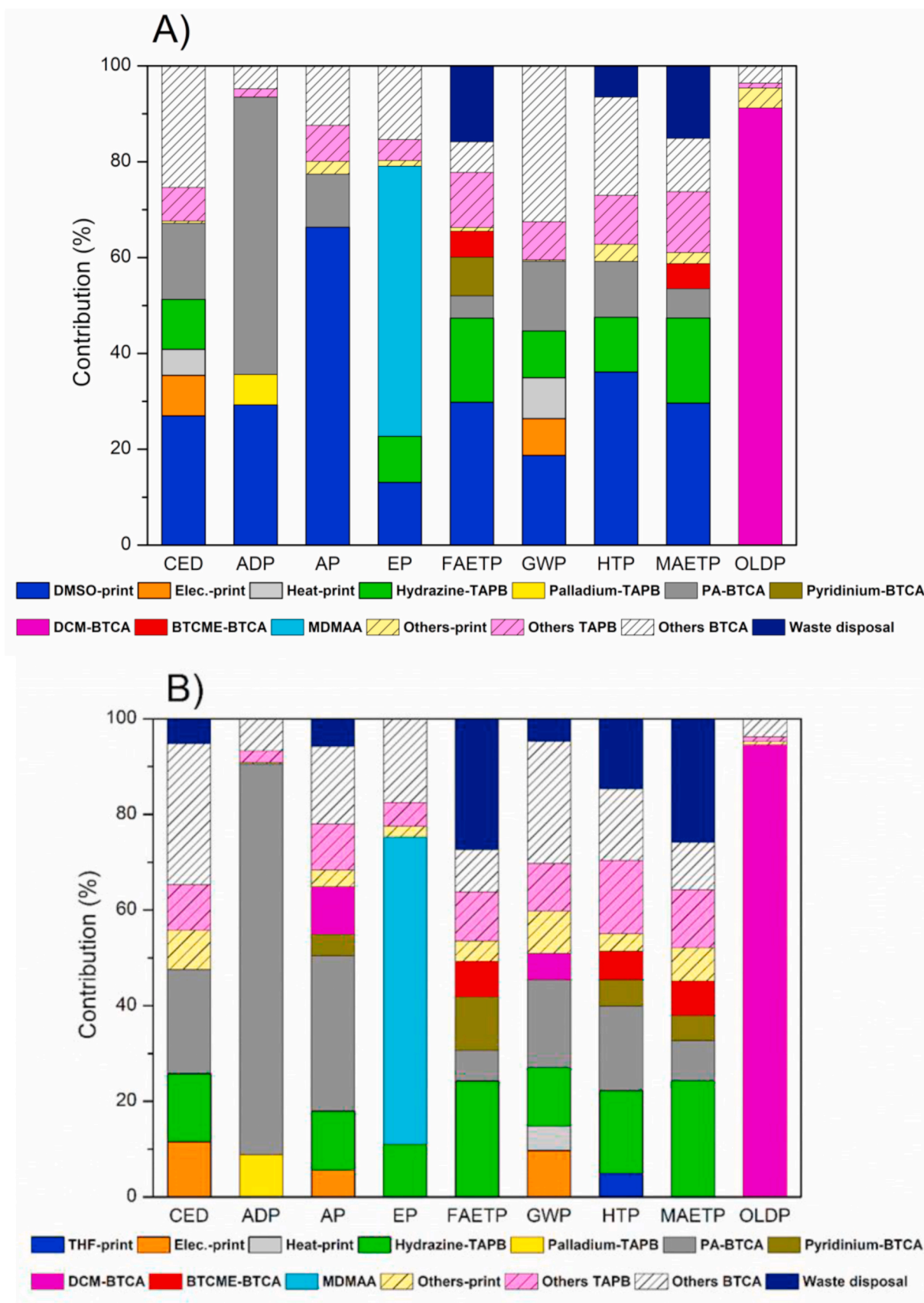
Fig. 4. Contribution process breakdown for inkjet printing processes: A) Case A and B) Case B.

66% and 11%, respectively). On the other hand, **PA** and hydrazine are the most important contributors in Case B (33 and 12%, respectively). In all cases, the impacts are due to acid emissions (mainly NOx and SO$_2$) produced in the manufacture of these compounds. With respect to **PA**, these emissions are generated from acetylene production because of the large amount required (>5g acetylene/g **BTCA** monomer).

The contribution analysis of EP category shows that the synthesis of **MDMAA** is the main responsible of this impact in both case studies (~ 60%) due to the high quantity of dimethylamine used for its synthesis (4.13 g dimethylamine/g **BTCA** monomer). This contribution is linked to inorganic emissions to fresh water (mainly ammonium and ammonia) generated by amine manufacture.

The processes with the highest contribution on FAETP are DMSO used in the printing process (~ 30%) and the hydrazine for **TAPB** synthesis (~ 18%) in Case A. This latter contribution is the largest in Case B (~ 25%). In all cases, the emission of heavy metals to fresh water during the production of DMSO and disposal of wastes generated in the synthesis of the hydrazine (due to the low yield of hydrazine synthesis) are the main responsible of these results.

The contribution to GWP is dominated by the production of DMSO (by 19%) and **PA** synthesis (by 15%) in Case A. Regarding to Case B, the main contributors are the synthesis of **PA** (by 22%) and hydrazine (by 12%). In the case of **PA**, the emissions produced in the acetylene and cooper catalyst manufacture are the responsible of these results, since large amount per gram of **BTCA** monomer (>5 in the case of acetylene and 1.5 for the catalyst) is needed. Finally, it can be observed in Fig. 4, how the rest of steps regarding to **BTCA** monomer synthesis (called others-**BTCA**) contributes by 30% in both Cases A and B. This value represents the largest contribution, but it must be noticed that it includes the sum of a wide number of single contributions (<5%) because **BTCA** synthesis involves a long supply chain from natural resources to the final monomer.

HTP category is affected by long-term emissions, especially heavy metals. As can be seen in Fig. 5, Case A shows as main contributors to this category DMSO manufacture (~ 36%) and synthesis of **PA** and hydrazine (~12%) involved in the synthesis of **TAPB** and **BTCA** monomers, respectively. These two latter contributions are the most important in Case B (~ 18%). In both case studies, emission of heavy metals to air produced by: DMSO manufacture, the construction of infrastructure for disposal of wastes (due to the low yield of hydrazine synthesis) and copper catalyst production (synthesis of **PA**) are responsible of these results.

Contribution results on MAETP category show that DMSO, hydrazine

synthesis and disposal of wastes produced by **BTCA** synthesis are the most important contributors (by 60%). As in the above category, the two latter contributions are the most important ones in Case B (sum by 40%). In all cases the heavy metals emitted to water are the responsible of these impacts.

Finally, regarding to OLDP category, it can be observed in Fig. 4, that dichloromethane used to obtain **MDMAA** (intermediate product in **BTCA** synthesis, as shown in Fig. 1) is clearly the most important contributor in both case studies (>90%). This result is consequence of halogenated organic compounds emitted to air by dichloromethane manufacture.

Overall, the use of DMSO in surface inkjet printing process, as well as the synthesis of **PA** and hydrazine needed for **BTCA** and **TAPB** synthesis, respectively, are the steps with the largest environmental burdens in most categories.

In order to check the possibility of reducing the most relevant impacts different alternatives were evaluated. The replacement of DMSO as solvent was previously explored by De la Peña Ruigómez et al. (2015). These authors identified *m*-cresol as a potential suitable solvent, but the printing process cannot be carried out (De la Peña Ruigómez et al. (2015). Regarding hydrazine synthesis, there is not an alternative route to obtain this compound (other precursors of hydrazine implies larger chain supply and therefore, they were dismissed). With respect to the synthesis of **PA** other routes were analysed to check their environmental feasibility.

The selected routes (shown in Fig. S4 of supplementary material) are based on synthesizing **PA** from propargyl alcohol, using glycerol (called PA-glycerol) or chloroallyl alcohol (PA-alcohol) as starting materials (Braun, 1936; Conant and Quayle, 1922). They were selected because one of them uses glycerol (which can be considered a waste from biofuel manufacture), whereas the other pathway is shorter than the acetylene-based route used in this work.

Both synthetic pathways were simulated, and the results used to quantify environmental impacts by LCA. These results were compared to those yielded by **PA** synthesis above explained, as depicted in Fig. 5. As can be observed, the synthesis based on acetylene is superior to the other ones in all categories, reducing dramatically the environmental impacts, except in ADP category due to a larger consumptions of element resources (mainly cooper). By analysing the syntheses based on glycerol and chloroallyl alcohol, it can be inferred that the former is superior. The main reason of this result is that the former uses chloropropene, which negatively affects the environmental impact of this synthesis pathway. Therefore, although the glycerol-based route uses a waste as starting material and the chloroallyl alcohol-based route requires less steps, none
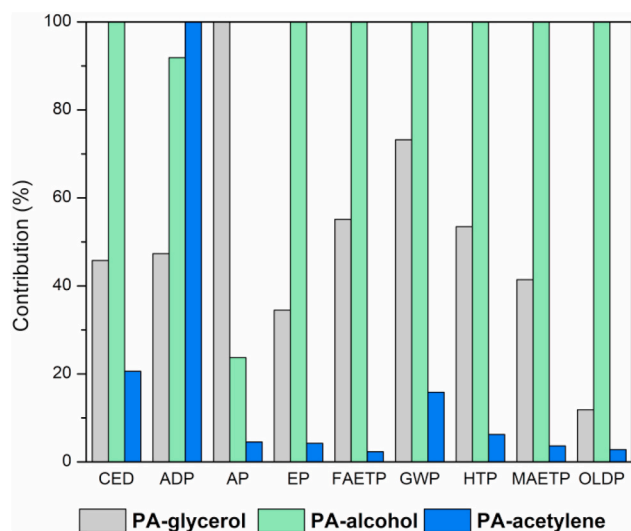

Fig. 5. Normalized comparison of LCA results for the studied synthesis pathways of **PA**.
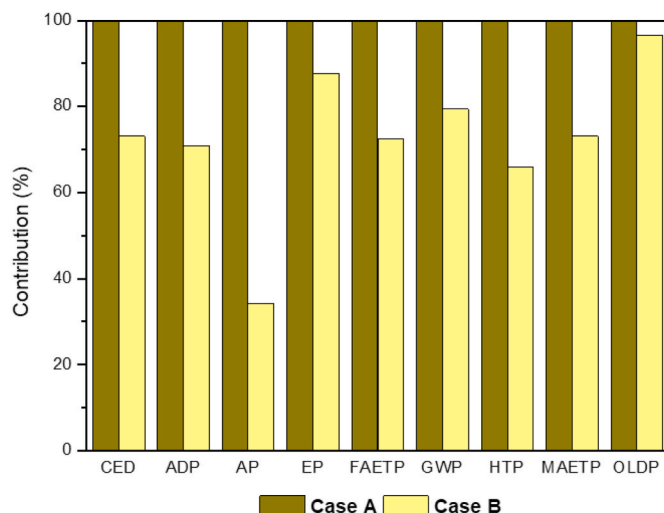

Fig. 6. Normalized comparison of LCA results for the case studies.

of them are superior to the synthesis based on acetylene.

3.3. Comparative analysis

In this section LCA results of Case A and B are compared. On the other hand, **RT-COF-1** is compared to other materials.

3.3.1. Comparison of case studies

Fig. 6 depicts the comparison between printing processes for Case A and B. As can be inferred, 3D inkjet printing (Case B) shows better results in all impact categories. As above explained, these results are directly related to the solvent used in the printing process (DMSO in Case A; and acetic acid in Case B). In this sense, it can be seen in Fig. 3 how the most important reductions are achieved in AP (by 65%), where the contribution of DMSO is the highest in Case A (see Fig. 3A). On the contrary, EP and OLDP categories are similar since the influence of DMSO is the lowest in both categories. For the rest of categories, reductions range between 25 and 35%. These results can be explained as impacts of DMSO manufacture are clearly higher than those of acetic acid production and besides, the amount used of the former is larger compared to that of the latter, as above commented. Therefore, Case B is superior to Case A from an environmental point of view.

3.3.2. Comparison between RT-COF-1 and other materials

Finally, LCA results of Case B are compared to data reported in the literature, as to our knowledge there are not LCA results on processes like Case A. For this purpose, LCA results reported by Maciel et al. (2019) for a PIL were used, as these authors use same impact categories and methodology for their quantification (Maciel et al., 2019). Nevertheless, both processes cannot be directly compared because of the assumptions to quantify LCA results were not the same, and therefore, the comparison should be taken with caution. In this sense, LCA results reported by Maciel et al. (2019) do not consider the end of wastes produced from the different processes, unlike our work, in which all wastes were assumed to be disposed as hazardous materials in an underground deposit. This point is relevant since this treatment affects notably to LCA results in the different categories, as explained in above sections. To make the results on **RT-COF-1** and PIL comparable, the impacts produced by waste disposal were subtracted from LCA results and they were supposed outputs of the different steps as *unspecified organic compounds*, in the same way as Maciel et al. (2019). Comparative results (normalized at 100%) are shown in Fig. 7, in which it can be observed how **RT-COF-1** is superior to PIL in five of nine categories (CED, ADP, AP, GWP and HTP), achieving impact reductions between 35% and >99%. These results, although must be taken with caution, allow us to confirm the potential of **RT-COF-1** as 3D-printing material from an environmental point of view. Nevertheless, research on more environmentally friendly routes (with higher efficiency and less harmful reactants) for **BTCA** synthesis as well as the reduction/substitution of solvents should be investigated.

4. Conclusions

Environmental impact of two inkjet printing methods (surface and 3D printing) using **RT-COF-1** were quantified by LCA approach. Synthesis of monomers to obtain **RT-COF-1** was the main contributor in both methods. On the other hand, the contribution of solvent used for surface printing was also noticeable. Regarding monomer contribution, **BTCA** was clearly larger than that of **TAPB** due to the longer chain supply (materials and energy) for its production. Specifically, the use of acetylene, **BTCA** precursor, and hydrazine synthesis needed to produce **TAPB** monomer are the most important contributors to the environmental impacts. The comparison between the studied cases reveals that using **RT-COF-1** for 3D printing is environmentally superior to surface printing because of less amount and lower hazardous solvents are needed. Comparison of LCA results on **RT-COF-1** with polymerizable
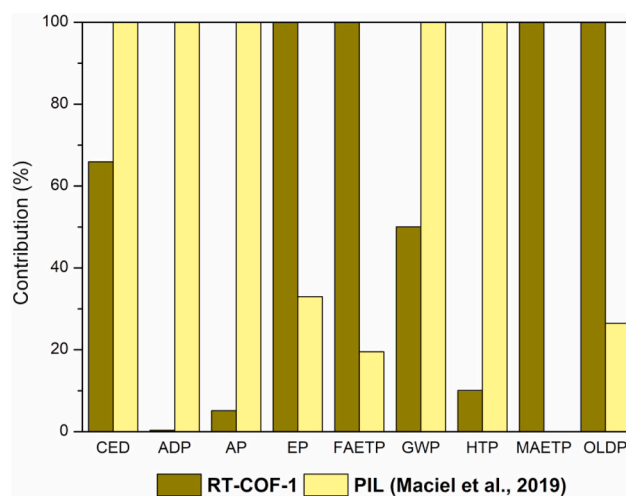

Fig. 7. Normalized comparison of LCA results for **RT-COF-1** (this work) and PIL (Maciel et al., 2019).

ionic liquids showed that this material is environmentally competitive for 3D-printing applications, exhibiting lower energy demand and carbon footprint, thus revealing its potential for this application. Nevertheless, this study is a first step that requires further research, mainly focused on optimizing synthesis of monomers and reducing the use of solvent, identifying the environmental hot spots concerning the application of COF-based materials in this field.

CRediT authorship contribution statement

Juan J. Espada: Conceptualization, Simulation and LCA work, Writing – original draft, preparation. **Rosalía Rodríguez:** Conceptualization, Writing – original draft, preparation. **Alejandro de la Peña:** Conceptualization, Writing – original draft, preparation. **Mar Ramos:** Formal analysis, Supervision. **José L. Segura:** Formal analysis, Supervision. **Esther M. Sánchez-Carnerero:** Conceptualization, Simulation work, Writing – original draft, preparation.

Declaration of competing interest

The authors declare that they have no known competing financial interests or personal relationships that could have appeared to influence the work reported in this paper.

Data availability

The authors are unable or have chosen not to specify which data has been used.

Appendix A. Supplementary data

Supplementary data to this article can be found online at https://doi.org/10.1016/j.jclepro.2023.136381.

References

Adams, R., Brown, B.K., 1941. Hydrazine sulfate. Org. Synth. 1, 37. https://doi.org/10.15227/orgsyn.002.0037.

Agrawal, R., 2021. Sustainable material selection for additive manufacturing technologies: a critical analysis of rank reversal approach. J. Clean. Prod. 296, 126500 https://doi.org/10.1016/j.jclepro.2021.126500.

Arava, V.R., Malreddy, S., Thummala, S.R., 2011. Di and trimerization of acrylic reagents. Sch. Res. Libr. 3, 491–495.

Athanasopoulou, L., Bikas, H., Stavropoulos, P., 2018. Comparative well-to-wheel emissions assessment of internal combustion engine and battery electric vehicles. Procedia CIRP 78, 25–30. https://doi.org/10.1016/j.procir.2018.08.169.

Baldwin, J.E., Black, K.A., 1984. Complete kinetic analysis of thermal stereomutations among the eight 2,3-Dideuterio-2-(methoxymethyl)spiro[cyclopropane-1,1′-indenes]. J. Am. Chem. Soc. 106, 1029–1040. https://doi.org/10.1021/ja00316a036.

Bao, C., Lu, R., Jin, M., Xue, P., Tan, C., Xu, T., Liu, G., Zhao, Y., 2006. Helical stacking tuned by alkoxy side chains in π-conjugated triphenylbenzene discotic derivatives. Chem. Eur J. 12, 3287–3294. https://doi.org/10.1002/chem.200501058.

Bikas, H., Lianos, A.K., Stavropoulos, P., 2019. A design framework for additive manufacturing. Int. J. Adv. Manuf. Technol. 103, 3769–3783. https://doi.org/10.1007/s00170-019-03627-z.

Braun, G., 1936. Epichlorohydrin and Epibromohydrin. Org. Synth. 16, 30. https://doi.org/10.15227/orgsyn.016.0030.

Cerdas, F., Juraschek, M., Thiede, S., Herrmann, C., 2017. Life cycle assessment of 3D printed products in a distributed manufacturing system. J. Ind. Ecol. 21, S80–S93. https://doi.org/10.1111/jiec.12618.

Cline, E.L., Emmet Reid, E., 1927. Some derivatives of ethylbenzene. J. Am. Chem. Soc. 49, 3150–3156.

Colson, J.W., Mann, J.A., Deblase, C.R., Dichtel, W.R., 2015. Patterned growth of oriented 2D covalent organic framework thin films on single-layer graphene. Polym. Chem. 53, 378–384. https://doi.org/10.1002/pola.27399.

Colson, J.W., Woll, A.R., Mukherjee, A., Levendorf, M.P., Spitler, E.L., Shields, V.B., Spencer, M.G., Park, J., Dichtel, W.R., 2011. Oriented 2D covalent organic framework thin films on single-layer graphene. Science 332, 228–232.

Conant, J.B., Quayle, O.R., 1922. Glyercol α,γ-dichlorohydrin. Org. Synth. 2, 29. https://doi.org/10.15227/orgsyn.002.0029.

Corey, E.J., Suggs, J.W., 1975. Pyridinium chlorochromate. An efficient reagent for oxidation of primary and secondary alcohols to carbonyl compounds. Tetrahedron Lett. 16, 2647–2650. https://doi.org/10.1016/S0040-4039(00)75204-X.

Côté, A.P., Benin, A.I., Ockwig, N.W., O'Keeffe, M., Matzger, A.J., Yaghi, O.M., 2005. Porous, crystalline, covalent porous, crystalline, covalent organic. frameworks 310, 1166–1170. https://doi.org/10.1126/science.1120411.

De la Peña Ruigómez, A., Rodríguez-San-Miguel, D., Stylianou, K.C., Cavallini, M., Gentili, D., Liscio, F., Milita, S., Roscioni, O.M., Ruiz-González, M.L., Carbonell, C., Maspoch, D., Mas-Ballesté, R., Segura, J.L., Zamora, F., 2015. Direct on-surface patterning of a crystalline laminar covalent organic framework synthesized at room temperature. Chem. Eur J. 21, 10666–10670. https://doi.org/10.1002/chem.201501692.

Díaz Velázquez, H., Wu, Z.X., Vandichel, M., Verpoort, F., 2017. Inserting CO2 into terminal alkynes via bis-(NHC)-Metal complexes. Catal. Lett. 147, 463–471. https://doi.org/10.1007/s10562-016-1920-5.

Diercks, C.S., Yaghi, O.M., 2017. The atom, the molecule, and the covalent organic framework. Science 355, 923–931. https://doi.org/10.1126/science.aal1585.

El-Kaderi, H.M., Hunt, J.R., Mendoza-Cortes, J.L., Cote, A.P., Taylor, R.E., O'Keeffe, M., Yaghi, O.M., 2007. Designed synthesis of 3D covalent organic frameworks. Science 316, 268–273. https://doi.org/10.1126/science.1139915.

Emerson, W.S., Heyd, J.W., Lucas, V.E., Stevenson, J.K., Wills, T.A., 1946. O-and p-Nitroacetophenones by liquid phase oxidation. J. Chem. Soc. 69, 706.

Espada, J.J., Villalobos, H., Rodríguez, R., 2021. Environmental assessment of different technologies for bioethanol production from Cynara cardunculus: a Life Cycle Assessment study. Biomass Bioenergy 144. https://doi.org/10.1016/j.biombioe.2020.105910.

Data sheet of DMP-2831 [WWW Document]. URL Fujifilm, 2013, last access 05/12/2022). https://tmi.utexas.edu/images/pdfs/fujifilm-cartridge-information.pdf.

Geng, K., He, T., Liu, R., Dalapati, S., Tan, K.T., Li, Z., Tao, S., Gong, Y., Jiang, Q., Jiang, D., 2020. Covalent organic frameworks: design, synthesis, and functions. Chem. Rev. 120, 8814–8933. https://doi.org/10.1021/acs.chemrev.9b00550.

Guan, X., Chen, F., Fang, Q., Qiu, S., 2020. Design and applications of three dimensional covalent organic frameworks. Chem. Soc. Rev. 49, 1357–1384. https://doi.org/10.1039/c9cs00911f.

Huijbregts, M.A.J., Hellweg, S., Frischknecht, R., Hendriks, H.W.M., Hungerbühler, K., Hendriks, J., 2010. Cumulative Energy Demand as Predictor for the Environmental Burden of Commodity Production, vol. 44, pp. 2189–2196.

Irlapati, N.R., Baldwin, J.E., Adlington, R.M., Pritchard, G.J., Cowley, A., 2003. An unusual oxidative cyclization: studies towards the biomimetic synthesis of pyridomacrolidin. Org. Lett. 5, 2351–2354. https://doi.org/10.1021/ol034736n.

Karami, Z., Soleimani-Gorgan, A., Vakili-Nezhaad, G.R., Roghabadi, F.A., 2022. A layer-by-layer green inkjet printing methodology for developing indium tin oxide (ITO)-based transparent and conductive nanofilms. J. Clean. Prod. 379, 134455 https://doi.org/10.1016/j.jclepro.2022.134455.

Khosravani, M.R., Reinicke, T., 2020. On the environmental impacts of 3D printing technology. Appl. Mater. Today 20, 100689. https://doi.org/10.1016/j.apmt.2020.100689.

Li, Y., Chen, W., Xing, G., Jiang, D., Chen, L., 2020. New synthetic strategies toward covalent organic frameworks. Chem. Soc. Rev. 49, 2845–3234. https://doi.org/10.1039/d0cs00199f.

Ma, J., Harstvedt, J.D., Dunaway, D., Bian, L., Jaradat, R., 2018. An exploratory investigation of Additively Manufactured Product life cycle sustainability assessment. J. Clean. Prod. 192, 55–70. https://doi.org/10.1016/j.jclepro.2018.04.249.

Maciel, V.G., Wales, D.J., Seferin, M., Sans, V., 2019. Environmental performance of 3D-Printing polymerisable ionic liquids. J. Clean. Prod. 214, 29–40. https://doi.org/10.1016/j.jclepro.2018.12.241.

Medina, D.D., Werner, V., Auras, F., Tautz, R., Dogru, M., Linke, S., Do, M., Feldmann, J., Knochel, P., Bein, T., 2014. Oriented thin films of a benzodithiophene covalent organic framework. ACS Nano 4, 4042–4052.

Mohammed, A.K., Usgaonkar, S., Kanheerampockil, F., Karak, S., Halder, A., Tharkar, M., Addicoat, M., Ajithkumar, T.G., Banerjee, R., 2020. Connecting microscopic structures, mesoscale assemblies, and macroscopic architectures in 3D-printed hierarchical porous covalent organic framework foams. J. Am. Chem. Soc. 142, 8252–8261. https://doi.org/10.1021/jacs.0c00555.

Muñoz, I., Alonso-Madrid, J., Menéndez-Muñiz, M., Uhart, M., Canou, J., Martin, C., Fabritius, M., Calvo, L., Poudelet, L., Cardona, R., Lombois-Burger, H., Vlasopoulos, N., Bouyssou, C., Dirrenberger, J., Papacharalampopoulos, A., Stavropoulos, P., 2021. Life cycle assessment of integrated additive–subtractive concrete 3D printing. Int. J. Adv. Manuf. Technol. 2149–2159. https://doi.org/10.1007/s00170-020-06487-0.

Okoroafor, T., Maalouf, A., Oez, S., Babu, V., Wilk, B., Resalati, S., 2022. Life cycle assessment of inkjet printed perovskite solar cells. J. Clean. Prod. 373, 133665 https://doi.org/10.1016/j.jclepro.2022.133665.

Panagiotopoulou, V.C., Stavropoulos, P., Chryssolouris, G., 2022. A critical review on the environmental impact of manufacturing: a holistic perspective. Int. J. Adv. Manuf. Technol. 118, 603–625. https://doi.org/10.1007/s00170-021-07980-w.

Rodríguez-San-Miguel, D., Zamora, F., 2019. Processing of covalent organic frameworks: an ingredient for a material to succeed. Chem. Soc. Rev. 48, 4375. https://doi.org/10.1039/c9cs00258h.

Rodríguez, R., Espada, J.J., Gallardo, M., Molina, R., López-Muñoz, M.J., 2018. Life cycle assessment and techno-economic evaluation of alternatives for the treatment of wastewater in a chrome-plating industry. J. Clean. Prod. 172, 2351–2362. https://doi.org/10.1016/j.jclepro.2017.11.175.

Saade, M.R.M., Yahia, A., Amor, B., 2020. How has LCA been applied to 3D printing? A systematic literature review and recommendations for future studies. J. Clean. Prod. 244, 118803 https://doi.org/10.1016/j.jclepro.2019.118803.

Shimizu, S., Abe, N., Iguchi, A., Dohba, M., Sato, H., Hirose, K.I., 1998. Synthesis of pyridine bases on zeolite catalyst. Microporous Mesoporous Mater. 21, 447–451. https://doi.org/10.1016/S1387-1811(98)00052-3.

Stavropoulos, P., Giannoulis, C., Papacharalampopoulos, A., Foteinopoulos, P., Chryssolouris, G., 2016. Life cycle analysis: comparison between different methods and optimization challenges. Procedia CIRP 41, 626–631. https://doi.org/10.1016/j.procir.2015.12.048.

Stavropoulos, P., Panagiotopoulou, V.C., 2022. Carbon Footprint of Manufacturing Processes: Conventional vs. Non-conventional, vol. 10. https://doi.org/10.3390/pr10091858.

Teo, M.Y., Kee, S., RaviChandran, N., Stuart, L., Aw, K.C., Stringer, J., 2020. Enabling free-standing 3D hydrogel microstructures with microreactive inkjet printing. ACS Appl. Mater. Interfaces 12, 1832–1839. https://doi.org/10.1021/acsami.9b17192.

Teo, M.Y., Kee, S., Stuart, L., Stringer, J., Aw, K.C., 2021. Printing of covalent organic frameworks using multi-material in-air coalescence inkjet printing technique. J. Mater. Chem. C 9, 12051–12056. https://doi.org/10.1039/d1tc03189a.

Wang, H., Zeng, Z., Xu, P., Li, L., Zeng, G., Xiao, R., Tang, Z., Huang, D., Tang, L., Lai, C., Jiang, D., Liu, Y., Qin, L., Ye, S., Ren, X., Tang, W., 2019. Recent progress in covalent organic framework thin films: fabrications, applications and perspectives. Chem. Soc. Rev. 48, 488. https://doi.org/10.1039/c8cs00376a.

Xu, X.Q., Wang, Z., Li, R., He, Y., Wang, Y., 2018. A degradable and recyclable photothermal conversion polymer. Chem. Eur J. 24, 9769–9772. https://doi.org/10.1002/chem.201801654.

Zawadzki, M., Zawada, K., Kowalczyk, S., Plichta, A., Jaczewski, J., Zabielski, T., 2022. 3D reactive inkjet printing of aliphatic polyureas using in-air coalescence technique. RSC Adv. 12, 3406–3415. https://doi.org/10.1039/d1ra07883f.